Electrical Power and Energy Systems 154 (2023) 109434

Contents lists available at ScienceDirect

International Journal of Electrical Power and Energy Systems

journal homepage: www.elsevier.com/locate/ijepes

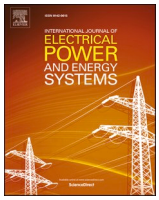

Mobile compressed air energy storage for active distribution systems

Mojtaba Jabbari Ghadi [a], Dillip Kumar Mishra [b,*], Ali Azizivahed [a], Li Li [a], Jiangfeng Zhang [b]

[a] School of Electrical and Data Engineering, University of Technology, Sydney, NSW 2007, Australia
[b] Department of Automotive Engineering, Clemson University, Greenville, SC 29607, United States

ARTICLE INFO

Keywords:
Compressed air energy storage
Mobile storage technology
Active distribution systems
Grid operation

ABSTRACT

Efficient energy storage technology is one of the key elements to enhance the flexibility, economy, and security of the power system. With the continuous development of energy storage technology, containerized mobile energy storage is coming into view, which has offered promising opportunities to improve distribution network (DN) performances and grid operating factors against emergencies. This paper proposes the concept of mobile compressed air energy storage (CAES) for an electric DN. The movable air storage tanks with stored energy are transported by trucks and placed at some distribution nodes/buses to improve DN performance. To overcome routing challenges for trucks, the configuration of the grid is mapped on the urban region of the city of Sydney, Australia, using Google map's Application Programming Interface. This approach can accurately model distances between current and targeted locations, unavailability of tanks during traveling, route congestions, and fuel consumptions. A new heuristic mathematical method is proposed in this paper to convert the constraints of the mobile CAES (MCAES) model into feasible search spaces, which significantly improves the convergence quality and speed. Operating results for both stationary and mobile CAESs are presented and compared. The methodology is applied to IEEE 136-bus DN in addition to IEEE 33-bus DN to demonstrate the competence of MCAES for larger-scale grids in optimizing the total operating profit, active power loss, energy not supplied, and voltage stability index of the grid. The crucial application of the proposed model can deal with natural disasters to avoid large-scale power outages and, eventually, mitigate the power system damages.

1. Introduction

1.1. Background and scope

Small-scale compressed air energy storage (CAES) applications in distribution networks (DNs) are growing significantly because of their lower investment costs and longer life-cycle compared to other storage technologies. For the stationary form of CAESs, authors in [1] employ a distribution size CAES for participating in the day-ahead electricity market. In [2], CAES technology is incorporated in the optimal scheduling of a small energy hub to minimize risk from uncertainties associated with energy price, load demand, and solar irradiations. In [3], the reactive power capability of CAES is employed in the optimal operation of a DN, in which a bi-objective dynamic optimal power flow problem is formulated and solved by Nash bargaining and a second-order cone program. In [4], the authors propose a new configuration of a dispatchable compressed-air-assisted wind turbine for DNs, which is capable of improving the mechanical performances of the wind turbine and subsequently increasing its generation and dispatchability. A bi-level planning approach, considering the operation and spinning-reserve requirements of DNs, is offered in [5] for an islanded microgrid equipped with a CAES. Further, a multi-objective optimal scheduling method using CAES is discussed in [6], where a demand response (DR) program is also employed. In [7], the thermal modelling of small-scale CAES is employed in the energy market formulations to demonstrate its differences from large-scale CAES in regard to efficiency, thermal modelling of heat exchanger unit, and loss destruction during compression and expansion procedures.

Recently, the concept of a transportable storage system has been getting more attention in electric power research [8]. For example, an energy management system is developed in [9], which schedules transportable energy storage systems (TESSs) in the form of battery units in a DN to minimize the cost of the power import from the grid. There are a few critical factors that need to be considered while employing the TESS in the DN, such as capacity, regulation performance, energy density, reliability, and resiliency. TESS is a promising solution to improve

* Corresponding author at: Department of Automotive Engineering, Clemson University, SC, USA.
E-mail address: dkmishra@ieee.org (D.K. Mishra).

https://doi.org/10.1016/j.ijepes.2023.109434
Received 12 December 2022; Received in revised form 5 July 2023; Accepted 7 August 2023
Available online 15 August 2023

the flexibility of the DN and the conversion capacities of microgrids [10]. Regarding the performance regulation, TESS can effectively balance the energy market as a price-maker/price-taker and provide ancillary services to the DN [11,12]. Considering natural disasters and other extreme events, the TESS can play a crucial role in load restoration, thus improving the reliability and resiliency of DN [13]. Further, a planning-operation methodology is presented in [14] to allocate a single TESS in a DN for power loss minimization, voltage regulation, and energy arbitrage considering the life cycles (i.e., 3000) and dynamic capacity of the battery. For microgrid applications, the allocation of multiple TESSs to various microgrids is accomplished in [15] using a path-based greedy algorithm to minimize the operating cost of DN. A preference-incentive co-evolution technique for optimal power scheduling and reconfiguration of isolated microgrids equipped with shiftable loads is proposed, which exploits the maximum transport capabilities of TESSs [16]. For resiliency/reliability applications, authors in [17,18] proposed models for planning and operation of the TESSs to improve the resiliency/reliability of the grid after a disaster. Another study with the objective of resilience improvement for microgrids is provided in [19] to optimize the investment of TESSs in the first stage and determine their new locations after a disaster in the second stage. A reliability-oriented study is accomplished in [20] based on Markov models and Monte Carlo simulation to evaluate the impacts of TESSs in the islanding mode operation of DN. To enhance reliability and reduce vulnerability, authors in [21] proposed a risk-based network expansion model with the TESS organizing approach, leading to reduced load shedding in the wake of extreme events. For service restoration applications: a Monte Carlo simulation-based two-stage stochastic restoration is developed in [22] to improve grid resilience while minimizing total cost. Another service restoration methodology is developed in [23] by the involvement of four agents (i.e., load, DG, switch, and battery) while the impact of both stationary and mobile storage is developed. Finally, authors in [24] and [25] focus on the optimal determination of transportation routes. In [24], the time-location movement modeling of TESSs to minimize the daily operation cost of DN is studied. Then a similarly detailed analysis is done in [25] to model transit periods and moving distances of TESSs for power loss minimization based on a set of linear equations. In [26], a joint probabilistic constraints-based study was presented with proper routing and scheduling of TESS to manage the dynamic configuration for better resiliency.

According to the literature discussed above, the key research gaps in mobile energy storage are summarized as follows:

- The CAES has emerged as a promising solution for future sustainable development practices; however, mobile CAES has not been fully considered to deal with uncertainties, eventualities, and power shortages.
- Since mobile energy storage technology is new, there is a great challenge to deal with investment costs and life cycles of CAESs in DNs.
- The transportating time of the TESS tank is not considered. The route delay during TESS tank transportation can significantly affect the reliability of DN, and, accordingly, power system instability occurs. Eventually, it can increase the operation time, and service restoration can be affected.

1.1.1. Approach and contributions

Considering the inexpensive cost of CAES, this paper will employ mobile CAES technology to fill the aforementioned research gaps. To this end, the novelties and contributions of this paper are as follows:

- High investment costs and limited life cycles of mobile battery-based storage are considerable challenges for the widespread development of these systems. Hence, a novel concept of mobile CAES (MCAES) is proposed, which has less capital costs but longer lifespan than the battery technology. Additionally, since the air tanks have much lower costs than generators, more mobile air tanks than generators are deployed. Thus, MCAESs offer a larger storage size with a higher level of dispatchability compared to TESSs at the same investment cost, and MCAESs also have a lower level of uncertainty compared to the fleet of electric vehicles. Therefore, MCAESs deliver substantial improvements for key operating factors of the grid, including the profit improvement for the distribution system operator (DSO), active power loss, energy not supplied, and voltage stability index.
- In terms of the solution approach, a new heuristic-based technique is proposed to overcome deficiencies of traditional constraint handling methods by converting constraints-related MCAESs into feasible ranges. This scheme, which is based on a forward–backward sweep, determines an appropriate range for charging/charging of each generator by which solutions are mapped with their feasible ranges and, subsequently, significantly increases the convergence quality and speed. Additionally, a new solution coding is proposed in which a single matrix will represent both commitment and dispatch matrices. Therefore, a notable size reduction in the dimension of the solution space is achieved, which contributes to a further convergence speed enhancement. The proposed mathematical formulation and constraint handling models are valid and applicable for both mobile and stationary forms of CAES, making switching between the two forms of CAES operation possible.
- Determining traveling time for transportable storage units considering route delays is one of the biggest challenges for mobile storage technology. Several methods have been presented in the literature to calculate distances and offer a list of priorities involving delays due to road congestion. This paper firstly maps the studied IEEE testing grid on the map of Sydney. Then, the most optimal routes are accurately determined based on hourly historical data of transportation using Google Maps Application Programming Interface (API), which effectively solves to the complicated route modeling problem.

The rest of the paper is organized as follows: Section 2 provides detailed modeling of the proposed MCAES, distributed generations (DGs), and operational constraints of the grid. Case studies and results for three scenarios with different schemes of generation/storage participation are presented in Section 3. Finally, Section 4 draws a conclusion from the obtained results.

2. Problem formulation and mathematical modeling

In this section, the mathematical modeling of the proposed system is developed. As noted earlier, this paper solves the coordinated operational problem involving distribution systems, where solar units, dispatchable fuel-based DGs, and fixed and mobile storage units are considered. In the first part of the formulation, the mathematical model of the MCAES is presented, which includes different modes of storage (charging, discharging, and idle), the storage capacity of a tank, energy level, and the total hourly operation cost of a CAES. Further, the location matrix formation formulation is discussed. In the formulation, CAES constraint handling formation through forward and backward approaches is employed and tested. In addition, the mathematical expression of distributed generators and required constraints for the grid operations are derived. The objective function is to optimize the total operating profit, active power loss, energy not supplied, and voltage stability index of the grid. Then the proposed model is tested through IEEE 136-bus DN in addition to IEEE 33-bus DN to demonstrate the competence of MCAES for larger-scale grids.

2.1. Mobile compressed air energy storage

This paper proposes a new concept of CAES units with transportable storage tanks and stationary generator units. The CAES system includes

a certain number of mobile storage tanks $\mathscr{M}$ that can be charged or discharged at the location of generators, where generator units $\mathscr{G}$ are stationary and located at candidate power distribution buses. In fact, a generator unit can only operate when connecting to one of the storage tanks. Three operating modes, including charging $\mathscr{C}$ (i.e., air compressing process to store air into tanks), discharging $\mathscr{D}$ (i.e., air releasing process for power generation), and idle are considered for a CAES unit. Obviously, a mobile tank is unavailable for electricity generation when it is moving from one electric node/bus to another. Additionally, each operating hour from the scheduling horizon is broken into several sub-periods. Although a generator can be physically connected to several tanks simultaneously, it only can charge/discharge one of them during each sub-period, and other tanks remain idle. In addition, the number of mobile tanks in the proposed system can be much more than the number of generator units.

2.2. Mathematical modeling

The modeling of the proposed MCAES is detailed as follows:

$$V_{m,t,c}^{\mathscr{M},\mathscr{C}} = \alpha_c^{\mathscr{G},\mathscr{C}} P_{m,t,c}^{\mathscr{G},\mathscr{C}} \forall m, \forall t, \forall c \tag{1}$$

$$\mho_{m,c}^{\mathscr{G},\mathscr{C}} U_{m,t,c}^{\mathscr{G},\mathscr{C}} \le V_{m,t,c}^{\mathscr{M},\mathscr{C}} \le \Omega_{m,c}^{\mathscr{G},\mathscr{C}} U_{m,t,c}^{\mathscr{G},\mathscr{C}} \forall m, \forall t, \forall c \tag{2}$$

$$\Omega_{m,c}^{\mathscr{G},\mathscr{C}} = min\left(\rho_c^{\mathscr{G},\mathscr{C}}, \mathscr{g}_m^{\mathscr{M}}\right) \forall m, \forall c \tag{3}$$

$$\mho_{m,c}^{\mathscr{G},\mathscr{C}} = \sigma_c^{\mathscr{G},\mathscr{C}} \Omega_{m,c}^{\mathscr{G},\mathscr{C}} \forall m, \forall c \tag{4}$$

$$P_{m,t,c}^{\mathscr{G},\mathscr{D}} = a_c^{\mathscr{G},\mathscr{D}} V_{m,t,c}^{\mathscr{M},\mathscr{D}} \forall m, \forall t, \forall c \tag{5}$$

$$\mho_{m,c}^{\mathscr{G},\mathscr{D}} U_{m,t,c}^{\mathscr{G},\mathscr{D}} \le V_{m,t,c}^{\mathscr{M},\mathscr{D}} \le \Omega_{m,c}^{\mathscr{G},\mathscr{D}} U_{m,t,c}^{\mathscr{G},\mathscr{D}} \forall m, \forall t, \forall c \tag{6}$$

$$\Omega_{m,c}^{\mathscr{G},\mathscr{D}} = min\left(\rho_c^{\mathscr{G},\mathscr{D}}, \mathscr{g}_m^{\mathscr{M}}\right) \forall m, \forall c \tag{7}$$

$$\mho_{m,c}^{\mathscr{G},\mathscr{D}} = \sigma_c^{\mathscr{G},\mathscr{D}} \Omega_{m,c}^{\mathscr{G},\mathscr{D}} \forall m, \forall c \tag{8}$$

$$U_{m,t,c}^{\mathscr{G},\mathscr{C}} + U_{m,t,c}^{\mathscr{G},\mathscr{D}} \le 1 \forall m, \forall t, \forall c \tag{9}$$

$$1 \ge \sum_{m=1}^{\overline{\mathscr{N}}_{t,c}} \left(\left| V_{m,t,c}^{\mathscr{M},\mathscr{C}} \right| \Big/ \rho_c^{\mathscr{G},\mathscr{C}} + \left| V_{m,t,c}^{\mathscr{M},\mathscr{D}} \right| \Big/ \rho_c^{\mathscr{G},\mathscr{D}} \right) \forall t, \forall c \tag{10}$$

$$P_{t,c}^{\mathscr{G}} = \sum_{m=1}^{N_M} \left(P_{m,t,c}^{\mathscr{G},\mathscr{D}} - P_{m,t,c}^{\mathscr{G},\mathscr{C}} \right) \forall t, \forall c \tag{11}$$

$$V_{t,c}^{\mathscr{G}} = \sum_{m=1}^{N_M} \left(V_{m,t,c}^{\mathscr{M},arr} - V_{m,t,c}^{\mathscr{M},dep} \right) + \sum_{m=1}^{N_M} \left(V_{m,t,c}^{\mathscr{M},\mathscr{C}} - V_{m,t,c}^{\mathscr{M},\mathscr{D}} \right) \forall t, \forall c \tag{12}$$

$$S_{m,t+1}^{\mathscr{M}} = S_{m,t}^{\mathscr{M}} + \sum_{c \in C_B} \left(V_{m,t,c}^{\mathscr{M},\mathscr{C}} - V_{m,t,c}^{\mathscr{M},\mathscr{D}} \right) \forall m, \forall t \tag{13}$$

$$S_{m,min}^{\mathscr{M}} \le S_{m,t}^{\mathscr{M}} \le \mathscr{g}_m^{\mathscr{M}} \forall m, \forall t \tag{14}$$

$$S_{m,min}^{\mathscr{M}} = \left(1 - \mu_m^{\mathscr{M}}\right) \mathscr{g}_m^{\mathscr{M}} \forall m \tag{15}$$

$$S_0^{\mathscr{M}\mathscr{G}} = S_{N_T}^{\mathscr{M}\mathscr{G}} = \sum_{m=1}^{N_M} S_{m,ini} \tag{16}$$

$$S_0^{\mathscr{M}\mathscr{G}} = \sum_{m=1}^{N_M} S_{m,0}^{\mathscr{M}} \tag{17}$$

$$S_{N_T}^{\mathscr{M}\mathscr{G}} = \sum_{m=1}^{N_M} S_{m,N_T}^{\mathscr{M}} \tag{18}$$

$$OC_t^{\mathscr{G}} = \sum_{m=1}^{N_M} \sum_{c \in C_B} \sum_{t=1}^{N_T} \left(P_{m,t,c}^{\mathscr{G},\mathscr{C}} \phi_{t,c}^{\mathscr{G},\mathscr{C}} + P_{m,t,c}^{\mathscr{G},\mathscr{D}} \left(HR_c^{\mathscr{G},\mathscr{D}} H_{NG} + \phi_{t,c}^{\mathscr{G},\mathscr{D}} \right) \right) \forall t \tag{19}$$

$$P_{t,c}^{\mathscr{G},\Psi} = \sum_{m=1}^{\overline{\mathscr{N}}_{t,c}} P_{m,t,c}^{\mathscr{G},\mathscr{D}}, \Psi = \mathscr{C}, \mathscr{D} \forall m, \forall t, \forall c \tag{20}$$

$$FC_t^{\mathscr{M}} = \sum_{m=1}^{N_M - 1} d_{m,t}^{\mathscr{M}} F_m^{\mathscr{M}} \forall t \tag{21}$$

$$R^{\mathscr{M}\mathscr{G}} = \sum_{t=1}^{N_T} \sum_{c \in C_B} \left(P_{t,c}^{\mathscr{G},\mathscr{D}} \pi_t^{\mathscr{T},m} - P_{t,c}^{\mathscr{G},\mathscr{C}} \pi_t^{\mathscr{T},b} \right) - \sum_{t=1}^{N_T} \left(FC_t^{\mathscr{M}} + OC_t^{\mathscr{G}} \right) \tag{22}$$

In (1), $V_{m,t,c}^{\mathscr{M},\mathscr{C}}$ is the amount of compressed energy during charging mode flowing into mobile tank m, with $m \in \{1, 2, \cdots, N_M\}$, at candidate bus $c \in C_B = \{c_1, c_2, \cdots, c_{N_C}\}$ and time step $t \in \{1, 2, \cdots, N_T\}$, where one hour is chosen for the sampling time step. Notation $P_{m,t,c}^{\mathscr{G},\mathscr{C}}$ is the amount of power to be received by CAES from the grid for compression and $\alpha_c^{\mathscr{G},\mathscr{C}}$ is the power-to-energy conversion rate. The hourly amount of energy stored in each storage unit is limited by (2), in which the upper bound $\Omega_{m,c}^{\mathscr{G},\mathscr{C}}$ and lower bound $\mho_{m,c}^{\mathscr{G},\mathscr{C}}$ are defined in (3) and (4), respectively; $U_{m,t,c}^{\mathscr{G},\mathscr{C}}$ is a binary variable indicating charging status of the CAES (i.e., $U_{m,t,c}^{\mathscr{G},\mathscr{C}} = 1$ means that tank m is being charged at time t by the generator located at bus c, and $U_{m,t,c}^{\mathscr{G},\mathscr{C}} = 0$ means it is not charged). As opposed to stationary CAES units in which hourly charging/discharging rates are a share of total storage capacity, these rates are considerable, and the corresponding capacity in one hour can be even higher than the storage capacity of a tank in the case of MCAESs. Therefore, as indicated in (3), the maximum hourly compression capacity $\Omega_{m,c}^{\mathscr{G},\mathscr{C}}$ of a CAES is defined as the minimum between nominal energy compression rate $\rho_c^{\mathscr{G},\mathscr{C}}$ of the motor unit and energy storage capacity of m^{th} mobile tank $\mathscr{g}_m^{\mathscr{M}}$. To maintain stability of the unit during charging and prevent frequent short-time operation of the generator, a minimum charging rate $\mho_{m,c}^{\mathscr{G},\mathscr{C}}$ as a percent of maximum charging rate is defined in (4).

The electric power provided by the CAES unit located at candidate bus c during discharging mode $P_{m,t,c}^{\mathscr{G},\mathscr{D}}$ is calculated in (5), where $a_c^{\mathscr{G},\mathscr{D}}$ refers to discharging conversion rate and $V_{m,t,c}^{\mathscr{M},\mathscr{D}}$ is the energy required for the generation of the scheduled power. The energy conversion rates for charge and discharge procedures are a fixed value $\alpha_c^{\mathscr{G},\Psi} = 0.85; \Psi = \mathscr{C}, \mathscr{D}; \forall c$ [1]. Similar to the charging mode, the amount of energy provision during discharging mode has a minimum bound and a maximum bound due to physical limitations as in (6). As the discharging rate of the generator $\rho_c^{\mathscr{G},\mathscr{C}}$ is higher than the storage capacity of a mobile tank $\mathscr{g}_m^{\mathscr{M}}$, the upper discharging limit of units $\Omega_{m,c}^{\mathscr{G},\mathscr{D}}$ is formulated by (7). Noteworthy, running the generator during the discharge period needs minimum pressure. Therefore, a discharging stability rate $\sigma_c^{\mathscr{G},\mathscr{D}}$ is considered to determine the lower discharging bound $\mho_{m,c}^{\mathscr{G},\mathscr{D}}$, expressed in (8). Considering $U_{m,t,c}^{\mathscr{G},\mathscr{C}}$ and $U_{m,t,c}^{\mathscr{G},\mathscr{D}}$ as binary variables referring to on/off status of a generator during charging and discharging periods, respectively, one of the states of charging, discharging, and idle can be considered for a CAES based on (9) in each operating period. If both binary variables $U_{m,t,c}^{\mathscr{G},\mathscr{C}}$ and $U_{m,t,c}^{\mathscr{G},\mathscr{D}}$ equal zero value, the generator is neither charging nor discharging, and therefore, it is in the idle state.

Since $\overline{\mathscr{N}}_{t,c}$ mobile tanks with $\overline{\mathscr{N}}_{t,c} \le N_m$ are available during hour t at the location of bus c, the hour t of the scheduling horizon is divided into several timeslots indexed by $\bar{t} \in \{1, 2, \cdots, \overline{\mathscr{T}}_{t,c}\}$ so that a certain amount of time is allocated to each storage tank committing to the charging/discharging procedures of a specific bus (i.e., simply calculated by $V_{m,t,c}^{\mathscr{M},\mathscr{C}} / \rho_c^{\mathscr{G},\mathscr{C}}$ and $V_{m,t,c}^{\mathscr{M},\mathscr{D}} / \rho_c^{\mathscr{G},\mathscr{D}}$). Obviously, $\overline{\mathscr{N}}_{t,c}$ can change by proceeding from one hour to the next one, and the summation of these timeslots for each generator should be in the range of one hour as mathematically expressed in (10). It is assumed that the movement of a transportable tank and the start of its commitment to a new bus happen only at the beginning of a scheduled hour. Moreover, automatic shifting values are accomplished by changing the pipe connection between the generator unit and mobile tanks in the bus. The time required for these actions is negligible and not considered in this paper. Considering the positive sign for power generating of storage units and the negative sign for power

purchasing from the grid, the N_T hour power profile $P_{t,c}^{\mathscr{G}}$ of CAES units are determined in (11). The hourly energy available at the place of each CAES unit, $V_{t,c}^{\mathscr{G}}$, presented in (12) includes two core terms; first from arrival $V_{m,t,c}^{\mathscr{M},arr}$ and departure $V_{m,t,c}^{\mathscr{M},dep}$ of mobile tanks transferring energy among the candidate buses, second from charging/discharging energy as the result of power exchange with the grid that increases/decreases the energy level at the relevant bus. Finally, the energy level of the mobile tanks $S_{m,t+1}^{\mathscr{M}}$ in the next hour is calculated in (13) by having the current level of energy $S_{m,t}^{\mathscr{M}}$ and scheduled hourly amount of charging energy $V_{m,t,c}^{\mathscr{M},\mathscr{C}}$ calculated in (1) and discharging energy $V_{m,t,c}^{\mathscr{M},\mathscr{D}}$ calculated in (5). In this formula, $V_{m,t,c}^{\mathscr{M},\mathscr{C}}$ and $V_{m,t,c}^{\mathscr{M},\mathscr{D}}$ are non-zero only when the tank is connected at a particular bus c, and are zero for all other buses. The energy level in mobile banks, due to physical constraints, is bounded in (14) by a maximum value $\mathscr{S}_m^{\mathscr{M}}$ and a minimum value $S_{m,min}^{\mathscr{M}}$ (i.e., defined as a share $\left(1-\mu_m^{\mathscr{M}}\right)$ of maximum value in (15) where $\mu_m^{\mathscr{M}}$ is the depth of discharge and is assumed to be 0.95 in this paper). As indicated in (16), the amount of energy stored in the MCAES system in the first hour $S_0^{\mathscr{M}\mathscr{G}}$ (i.e., evaluated in (17)) and last hour $S_{N_T}^{\mathscr{M}\mathscr{G}}$ (i.e., evaluated in (18)) of scheduling need to be the same. Noteworthy, this value is lower than that for large-scale CAESs due to the lower thermal efficiency of the heat exchanger in small-scale CAESs. The total hourly operation cost of a CAES system $OC_t^{\mathscr{G}}$ is given in (19) where $\phi_{t,c}^{\mathscr{G},\mathscr{C}}$ and $\phi_{t,c}^{\mathscr{G},\mathscr{D}}$ are the variable operating costs of a CAES unit during charging/discharge modes, respectively. Considering a simple cycle mode for CAESs, $HR_c^{\mathscr{G},\mathscr{D}}$ refers to the fuel heat rate and H_{NG} is the price of natural gas for operating a gas turbine. However, an air turbine is employed instead of a gas turbine in the small-scale CAES systems; therefore, the operating cost can be considered as negligible value. As defined in (20), the total power generation $P_{m,t,c_i}^{\mathscr{G},\psi}$ of a generatorat a timestep t is calculated as the summation of its charge/discharge powers during sub-timestep $\bar{t}$. Besides, an hourly fuel cost $FC_t^{\mathscr{M}}$ is considered for moving tanks as formulated in (21) where $d_{m,t}^{\mathscr{M}}$ refers to km traveling distance between the bus location of a tank at time t and its bus location at the next hour, and $F_m^{\mathscr{M}}$ is per km fuel consumption of tank m. Finally, profit from the commitment of an MCAES system $R^{\mathscr{M}\mathscr{G}}$ is determined in (22) where electric power provided/demanded by storage is exchanged with the grid at the selling $\pi_t^{\mathscr{T},m}$/ purchasing $\pi_t^{\mathscr{T},b}$ price. This paper assumes that $\rho_c^{\mathscr{G},\psi} > \mathscr{S}_m^{\mathscr{M}}; \psi = \mathscr{C}, \mathscr{D} \forall m, \forall c$, which means the charge/discharge capacity of the generator is bigger than the capacity of each mobile tank.

2.3. Location matrix formation of mobile CAESs

In order to make the problem as realistic as possible, the location of buses of an IEEE DN is mapped on the urban area of the city of Sydney. The actual distances and time needed to travel between buses are based on 24 h historical data gathered from API. The following proposed algorithm modifies the randomly generated matrix of tanks' movements $\mathrm{M} = \left[\mathbb{C}_{i,j}\right]_{N_M \times N_T}$, and $\mathbb{C}_{i,j}$ is uniformly generated from integers $\{c_1, c_2, \cdots, c_{N_C}\}$. The N_M dimensional matrix M indicates that the bus location of each of the tanks during the N_T scheduling period. In other words, $\mathbb{C}_{i,j}$ shows the m^{th} tank is sitting at the location of the bus c_i at time t. Here the authors used lowercase for scalars, lowercase bold for vectors, capital bold for matrices, and double-lined capital letters for a matrix of randomly generated numbers in notations.

2.3.1. Initialization

Initialize the modified matrix of tank scheduling $\breve{\boldsymbol{M}} = \mathbf{M}$, the unavailability matrix of tanks $\mathscr{O} = \left[\mathbb{A}_{i,j}\right]_{N_M \times N_T}$, the required time for a truck to move from bus i to bus j $\Delta_{i,j} = \left\lceil \mathfrak{D}_{i,j}/\mathfrak{s} \right\rceil$, the location of mobile tanks at the first hour $\mathbb{C}_{i,1} = \lambda_i$, and $\mathscr{N}_M$ dimensional vector $\boldsymbol{\tau} = [\mathbb{A}_i]_{N_M}$ which indicates the number of idle hours for each tank; where $\mathbb{A}_{i,j}$ is generated with a value of zero, $\lceil \xi \rceil$ is the ceiling function which finds the least integer greater than or equal to ξ, $\mathfrak{D}_{i,j}$ is the distance between two individual buses i and j (i.e., calculated by Google Maps) in the unit of km and, $\mathfrak{s}$ is the speed of trucks carrying tanks (i.e., similar and constant), λ_i is ith row of the vector λ and the same as λ_m (i.e., pre-defined by math function $\mathbb{C}$), $\mathbb{A}_i$ is generated from an initial value 0 (i.e., there are no restrictions on operating hours from the previous day).

2.3.2. Loop calculation

For m from 1 to N_M, do the following:
Set variables $\vartheta = 1, t = 2, \varepsilon = \boldsymbol{\tau}_m$.
While t is less than $N_T + 1$, do the following:

1. Calculate scaler values of the current location $\mathscr{\ell}^{\mathscr{C}}$, next location $\mathscr{\ell}^{\mathscr{N}}$, and time distance θ:

$$\mathscr{\ell}^{\mathscr{C}} = \mathrm{M}_{m,\vartheta} \tag{23-a}$$

$$\mathscr{\ell}^{\mathscr{N}} = \mathrm{M}_{m,t} \tag{23-b}$$

$$\theta = \Delta_{\mathscr{\ell}^{\mathscr{C}},\mathscr{\ell}^{\mathscr{N}}} \tag{23-c}$$

where $\mathrm{M}_{m,\vartheta}$ is (m,ϑ) element of M, $\mathrm{M}_{m,t}$ is the (m,t) element of M, and $\Delta_{\mathscr{\ell}^{\mathscr{C}},\mathscr{\ell}^{\mathscr{N}}}$ is the $\left(\mathscr{\ell}^{\mathscr{C}},\mathscr{\ell}^{\mathscr{N}}\right)$ element of Δ.

2. Calculate elements of $\breve{\boldsymbol{M}}$ and $\mathscr{O}$ as follows:

$$\begin{cases} t = t+1, \ \varepsilon = \varepsilon + 1; & \text{if } \mathscr{\ell}^{\mathscr{C}} = \mathscr{\ell}^{\mathscr{N}} \\ \breve{\boldsymbol{M}}_{m,t} = \mathscr{\ell}^{\mathscr{C}}, \ t = t+1, \ \varepsilon = \varepsilon + 1; & \text{if } \theta > \varepsilon \\ \mathscr{O}_{m,t-\theta:\, t-1} = inf, \ \vartheta = t, \ t = t+1, \ \varepsilon = 0; & \text{if } \theta < \varepsilon \end{cases} \tag{23-d}$$

where $\breve{\boldsymbol{M}}$ is the scheduling matrix.

2.3.3. Final adjustment

Calculate the final scheduling matrix $\widetilde{\boldsymbol{M}}$:

$$\widetilde{\boldsymbol{M}}_{m,t} = \max\left(\breve{\boldsymbol{M}}_{m,t}, \ \mathscr{O}_{m,t}\right) \ \forall m, \ \forall t \tag{24}$$

where $\widetilde{\boldsymbol{M}}_{m,t}$ is the (m,t) element of $\widetilde{\mathbf{M}}$.

2.4. Proposed through

2.4.1. Forward approach

2.4.1.1. Initialization.

1. Initialize the energy scheduling matrix $\mathbf{S}^{\mathscr{M}} = \left[\mathbb{A}_{i,j}\right]_{N_M \times N_T}$ for tanks, as well as the initial amount $\mathbb{A}_{i,1} = \boldsymbol{s}_{i,ini}$ for the first hour; where $\boldsymbol{s}_{i,ini}$ is the ith row of $\boldsymbol{s}_{ini}$ (i.e., the same as $\boldsymbol{s}_{m,ini}$), $\mathrm{X}^{\mathscr{M}} = \left[\mathbb{C}_{i,j}\right]_{N_M \times N_T}$ is a decision matrix for energy scheduling of tanks with random values $\mathbb{C}_{i,j}$ from the interval $[0,1]$ while $\mathbb{C}_{i,j} = 0$ *if* $\mathscr{O}_{i,j} = inf$ (i.e., the value *inf* refers to the hours in which tanks are not available due to moving between buses).

2. Initialize charging/ discharging/ idle status of units $U^{\mathscr{G}}$ (i.e., $+1$, -1, 0) by using the sign function, as defined in (25-a); while $\mathbf{U}_{m,t}^{\mathscr{G}} = 0$ *if* $\mathscr{O}_{m,t} = inf$ which shows unavailability of units.

$$\mathbf{U}_{m,t}^{\mathscr{G}} = \begin{cases} +1 if \left(\mathrm{X}_{m,t}^{\mathscr{M}} - 0.5\right) \rangle 0 \\ 0 if \left(\mathrm{X}_{m,t}^{\mathscr{M}} - 0.5\right) = 0 \\ -1 if \left(\mathrm{X}_{m,t}^{\mathscr{M}} - 0.5\right) \langle 0 \end{cases} \tag{25-a}$$

3. Calculate the matrices charging state $\mathbf{U}_{m,t}^{\mathscr{G},\mathscr{C}} = \max(\mathbf{U}_{m,t}^{\mathscr{G}}, 0)$ and discharging state $\mathbf{U}_{m,t}^{\mathscr{G},\mathscr{D}} = -\min(\mathbf{U}_{m,t}^{\mathscr{G}}, 0)$.

4. Calculate the matrix $\mathrm{X}^{\mathscr{G},\varpi}$ in (25-b) as input for calculating energy charge/discharge of mobile tanks.

$$\mathrm{X}_{m,t}^{\mathscr{G},\varpi} = \left(2 \times \left(\mathrm{X}_{m,t}^{\mathscr{M}} - 0.5\right)\right)\mathbf{U}_{m,t}^{\mathscr{G},\varpi}\varpi = \mathscr{C}, \mathscr{D}\forall m, \forall \mathrm{t} \tag{25-b}$$

The term $\left(\mathrm{X}_{m,t}^{\mathscr{M}} - 0.5\right)$ scales all random values down within [−0.5, +0.5], in which positive/negative values refer to charging/ discharging. The term "×2″ maps them again within [−1, +1], and then, all values of matrices $\mathrm{X}^{\mathscr{G},\mathscr{C}}$ and $\mathrm{X}^{\mathscr{G},\mathscr{D}}$ are within [0, 1]. Noteworthy, both the commitment and dispatch states of units are detached from a single matrix.

2.4.1.2. Loop calculation. The first loop sets parameters for mobile tanks.

For $t$from1toN_T, do the following.

Set an hourly upper $\Delta_m^{\mathscr{M}}$ (lower $\mathbf{Y}_m^{\mathscr{M}}$) available capacity, energy charging/discharging percentage $\boldsymbol{\chi}_m^{\mathscr{G},\varpi}$ (i.e., still within the interval [0,1]), and the movement of each tank $\boldsymbol{\mu}_m$, where $\alpha_m^{\mathscr{M}}$ is the maximum depth of discharge of tanks.

$$\Delta_m^{\mathscr{M}} = \mathscr{g}_m^{\mathscr{M}} - \mathbf{S}_{m,t}^{\mathscr{M}} \ \forall m \tag{26-a}$$

$$\mathbf{Y}_m^{\mathscr{M}} = \mathbf{S}_{m,t}^{\mathscr{M}} - \left(\left(1 - \alpha_m^{\mathscr{M}}\right)\mathscr{g}_m^{\mathscr{M}}\right)\forall m \tag{26-b}$$

$$\boldsymbol{\chi}_m^{\mathscr{G},\varpi} = \mathrm{X}_{m,t}^{\mathscr{G},\varpi}\varpi = \mathscr{C}, \mathscr{D}\forall m \tag{26-c}$$

$$\boldsymbol{\mu}_m = \widetilde{\mathrm{M}}_{m,t}\forall m \tag{26-d}$$

The second loop calculates the energy amount of each tank

For $c$from the set $\{c_1, c_2, \cdots, c_{N_C}\}$, do the following.

$$\boldsymbol{k}_m = \begin{cases} 1 if \boldsymbol{\mu}_m = c \\ 0 if \boldsymbol{\mu}_m \neq c \end{cases}\forall m \tag{27-a}$$

$$\boldsymbol{v}_m^{\mathscr{M},\mathscr{C}\mathscr{D}} = \left(\boldsymbol{\chi}_m^{\mathscr{G},\mathscr{C}}\,\Delta_m^{\mathscr{M}} + \boldsymbol{\chi}_m^{\mathscr{G},\mathscr{D}}\,\mathbf{Y}_m^{\mathscr{M}}\right)\boldsymbol{k}_m\forall m \tag{27-b}$$

$$\widetilde{\boldsymbol{v}}_m^{\mathscr{M},\mathscr{C}\mathscr{D}} = \max\left(\min\left(\boldsymbol{v}_m^{\mathscr{M},\mathscr{C}\mathscr{D}}, \Omega_{m,c}^{\mathscr{G},\mathscr{C}}\right), -\Omega_{m,c}^{\mathscr{G},\mathscr{D}}\right)\forall m \tag{27-c}$$

$$\widetilde{\boldsymbol{v}}_m^{\mathscr{M},\mathscr{C}\mathscr{D}} = \begin{cases} 0 \ \text{ if } \ \widetilde{\boldsymbol{v}}_m^{\mathscr{M},\mathscr{C}\mathscr{D}} > 0 \,\&\, \widetilde{\boldsymbol{v}}_m^{\mathscr{M},\mathscr{C}\mathscr{D}} < \mho_{m,c}^{\mathscr{G},\mathscr{C}} \\ 0 \ \text{ if } \ \widetilde{\boldsymbol{v}}_m^{\mathscr{M},\mathscr{C}\mathscr{D}} < 0 \,\&\, \widetilde{\boldsymbol{v}}_m^{\mathscr{M},\mathscr{C}\mathscr{D}} > -\mho_{m,c}^{\mathscr{G},\mathscr{D}} \end{cases} \tag{27-d}$$

where $\boldsymbol{k}$ indicates available/unavailable tanks at bus c_i (i.e., the place of the selected generator), and $\boldsymbol{v}_m^{\mathscr{M},\mathscr{C}\mathscr{D}}$ is the amount of energy charging/ discharging of the mobile tanks. Currently, none of the generated solutions violate the constraints except Eq. (10), which is met by the following *IF* condition.

$$\mathscr{k} = \sum_{m=1}^{N_M}\left(\frac{\widetilde{\boldsymbol{v}}_m^{\mathscr{M},\mathscr{C}\mathscr{D}}\,\mathrm{i}_{\boldsymbol{m}}^{\mathscr{M},\mathscr{C}}}{\rho_c^{\mathscr{G},\mathscr{C}}} + \frac{\widetilde{\boldsymbol{v}}_m^{\mathscr{M},\mathscr{C}\mathscr{D}}\,\mathrm{i}_{\boldsymbol{m}}^{\mathscr{M},\mathscr{D}}}{\rho_c^{\mathscr{G},\mathscr{D}}}\right)\forall m \tag{28-e}$$

$$\mathrm{i}_{\boldsymbol{m}}^{\mathscr{M},\mathscr{C}} = \begin{cases} 1 if \widetilde{\boldsymbol{v}}_m^{\mathscr{M},\mathscr{C}\mathscr{D}} > 0 \\ 0 if otherwise \end{cases}\forall m \tag{28-f}$$

$$\mathrm{i}_{\boldsymbol{m}}^{\mathscr{M},\mathscr{D}} = \begin{cases} 1 if \widetilde{\boldsymbol{v}}_m^{\mathscr{M},\mathscr{C}\mathscr{D}} < 0 \\ 0 if otherwise \end{cases}\forall m \tag{28-g}$$

where $\mathscr{k}$ is the total operating hour of a generator, and $\mathrm{i}_{\boldsymbol{m}}^{\mathscr{M},\mathscr{C}}$ ($\mathrm{i}_{\boldsymbol{m}}^{\mathscr{M},\mathscr{D}}$) is a charging (discharging) binary index.

If $\mathscr{k}$ is greater than 1, do the following:

$$\mathscr{r}_m^{\mathscr{G},\mathscr{C}\mathscr{D}} = (\mathscr{k} - 1)\frac{\widetilde{\boldsymbol{v}}_m^{\mathscr{M},\mathscr{C}\mathscr{D}}}{\sum_{m=1}^{N_M}\left|\widetilde{\boldsymbol{v}}_m^{\mathscr{M},\mathscr{C}\mathscr{D}}\right|}\forall m \tag{29-a}$$

$$\mathbf{V}_{m,t}^{\mathscr{M},\mathscr{C}\mathscr{D}} = \widetilde{\boldsymbol{v}}_m^{\mathscr{M},\mathscr{C}\mathscr{D}} - \left(\rho_c^{\mathscr{G},\mathscr{C}}\left(\mathscr{r}_m^{\mathscr{G},\mathscr{C}\mathscr{D}}\mathrm{i}_{\boldsymbol{m}}^{\mathscr{M},\mathscr{C}}\right) - \rho_c^{\mathscr{G},\mathscr{D}}\left(\left|\mathscr{r}_m^{\mathscr{G},\mathscr{C}\mathscr{D}}\right|\mathrm{i}_{\boldsymbol{m}}^{\mathscr{M},\mathscr{D}}\right)\right)\forall m \tag{29-b}$$

where $\mathscr{r}_m^{\mathscr{G},\mathscr{C}\mathscr{D}}$ is the percentage of required decrements.

Otherwise

Set the final dispatch as $\mathbf{V}_{m,t}^{\mathscr{M},\mathscr{C}\mathscr{D}} = \widetilde{\boldsymbol{v}}_m^{\mathscr{M},\mathscr{C}\mathscr{D}}\ \forall m$.

2.4.1.3. Final adjustment. Finally, update the existing energy of tanks in (30)).

$$\mathbf{S}_{m,t+1}^{\mathscr{M}} = \mathbf{S}_{m,t}^{\mathscr{M}} + \mathbf{V}_{m,t}^{\mathscr{M},\mathscr{C}\mathscr{D}}\ \forall m \tag{30}$$

2.4.2. Backward approach

The backward approach modifies $\mathbf{V}_{m,t}^{\mathscr{M},\mathscr{C}\mathscr{D}}$ to meet Eq. (16).

2.4.2.1. Loop calculation. For decreasing counter $t$from$N_T$to1, do the following.

Set the vector $\boldsymbol{\eta} = [\mathbb{A}_{\mathrm{i}}]_{N_M}$, as an indicator of generators that reach their maximum operating capacity.

While ($|\mathscr{g}|$ is less than$\epsilon^{\mathscr{g}}$) or ($\eth$is greater than$\epsilon^{\eth}$), do the following:

$$\mathbf{S}_{m,t}^{\mathscr{M}} = \sum_{j=1}^{t}\boldsymbol{s}_{m,ini}\,\mathbf{V}_{m,j}^{\mathscr{M},\mathscr{C}\mathscr{D}}, \forall m, \forall t \tag{31-a}$$

$$\mathscr{g} = \sum_{m=1}^{N_M}\boldsymbol{s}_{m,ini} - \sum_{m=1}^{N_M}\mathbf{S}_{m,N_T}^{\mathscr{M}} \tag{31-b}$$

$$\widetilde{\Delta}_m^{\mathscr{M}} = \Delta_m^{\mathscr{M}}(1\text{-}\boldsymbol{\eta}_m), \forall m, \tag{31-c}$$

$$\widetilde{\mathbf{Y}}_m^{\mathscr{M}} = \mathbf{Y}_m^{\mathscr{M}}(1\text{-}\boldsymbol{\eta}_m), \ \forall m \tag{31-d}$$

where $\mathscr{g}$ is the energy surplus/shortage, $\epsilon^{\mathscr{g}}$ is a user-defined termination criterion for energy mismatch, $\eth$ is an iteration counter, $\epsilon^{\eth}$ is a user-defined termination criterion for the counter $\eth$, $\widetilde{\Delta}_m^{\mathscr{M}}$ and $\widetilde{\mathbf{Y}}_m^{\mathscr{M}}$ are modified available capacities. Then, the index $\boldsymbol{\eta}$ is reset to zero $\boldsymbol{\eta}_m = 0\ \forall m$.

To calculate units' dispatch share from energy surplus:

$$\boldsymbol{\varphi}_m = \begin{cases} 1 if \boldsymbol{\mu}_m = inf \\ 0 if \boldsymbol{\mu}_m \neq inf \end{cases}, \ \forall m \tag{31-e}$$

$$\varnothing_m = \begin{cases} -\dfrac{\widetilde{\mathbf{Y}}_m^{\mathscr{M}}\boldsymbol{\varphi}_m}{\sum_{m=1}^{\mathscr{N}_M}\left(\widetilde{\mathbf{Y}}_m^{\mathscr{M}}\boldsymbol{\varphi}_m\right)}|\mathscr{g}| if \mathscr{g} > 0 \\ +\dfrac{\widetilde{\Delta}_m^{\mathscr{M}}\boldsymbol{\varphi}_m}{\sum_{m=1}^{\mathscr{N}_M}\left(\widetilde{\Delta}_m^{\mathscr{M}}\boldsymbol{\varphi}_m\right)}|\mathscr{g}| if \mathscr{g} \leq 0 \end{cases}, \forall m, \tag{31, -f}$$

where the index $\boldsymbol{\varphi}_m$ indicates whether tanks are available at the location of a candidate. Then, firstly set a temporary variable $\epsilon_m = \mathbf{V}_{m,t}^{\mathscr{M},\mathscr{C}\mathscr{D}}\forall m$ and $\mathbf{V}_{m,t}^{\mathscr{M},\mathscr{C}\mathscr{D}} = 0\,\forall m$; after that, define the share of units from energy surplus/shortage $\varnothing_m$:

For c from the set $\{c_1, c_2, \cdots, c_{N_C}\}$, do the following:

$$\boldsymbol{v}_m^{\mathscr{M},\mathscr{C}\mathscr{D}} = \left(\boldsymbol{v}_m^{\mathscr{M},\mathscr{C}\mathscr{D}} + \varnothing_m\right)\boldsymbol{k}_m, \ \forall m \tag{32}$$

Similar to the forward approach, apply Eqs. (27-c) and (27-d) to $\boldsymbol{v}_m^{\mathscr{M},\mathscr{C}\mathscr{D}}$ to reach the constrained dispatch $\widetilde{\boldsymbol{v}}_m^{\mathscr{M},\mathscr{C}\mathscr{D}}$. Then, calculate $\mathscr{k}$ and evaluate the following IF condition; otherwise $\mathbf{V}_{m,t}^{\mathscr{M},\mathscr{C}\mathscr{D}} = \widetilde{\boldsymbol{v}}_m^{\mathscr{M},\mathscr{C}\mathscr{D}}\ \forall m$.

If $\mathscr{k}$ is greater than 1, do the following:

As same as the forward approach, Eqs. (29-a) and (29-b) are used to

modify the current violated solution. Since some units reach their maximum or minimum capacity within the condition of While loop in the backward approach, the variable $\boldsymbol{\eta}_m$ is updated as in (33).

$$\boldsymbol{\eta}_m = \boldsymbol{\eta}_m + \dot{\imath}_{\boldsymbol{m}}^{\mathscr{M},\mathscr{C}} + \dot{\imath}_{\boldsymbol{m}}^{\mathscr{M},\mathscr{D}},\ \forall m \tag{33}$$

At this stage, the final energy charge/discharge of selected tanks is updated as $\mathbf{V}_{m,t}^{\mathscr{M},\mathscr{C}\mathscr{D}} = \widetilde{\boldsymbol{v}}_m^{\mathscr{M},\mathscr{C}\mathscr{D}}\ \forall m$.

2.4.2.2. Final adjustment. Then, $\eth = \eth + 1$ and $\mathscr{g}$ is recalculated in (31-b); if one of the termination conditions is met, the While loop is terminated.

2.5. Distributed generators

The DN needs DGs to participate in the operation of the grid to improve operational factors or to help the DSO to implement a secure operation. To this end, solar units and fuel-based dispatchable DGs are modelled in this paper.

2.5.1. Solar units

For solar units, the generation of units is assumed constant during each hour of scheduling and is also non-dispatchable. The detailed specifications of these units (i.e., including generation pattern, location, and capacity) are presented in the case study section. Given the hourly power generation of the solar photovoltaic (PV) unit $P_{\mathscr{g},t}^{\mathscr{G}}$ where $\mathscr{g} \in \{1,2,\ldots,N_Y\}$, and considering the operating cost of PV generation a negligible value, the revenue (i.e., equal to profit) of the solar system is calculated in (34):

$$R^{\mathscr{G}} = \sum_{t=1}^{N_T}\sum_{\mathscr{a}=1}^{N_Y} P_{\mathscr{g},t}^{\mathscr{G}} \pi_t^{\mathscr{S},m} \tag{34}$$

2.5.2. Fuel-based distributed generation units

The model of dispatchable fuel-based DGs is as follows:

$$\mho_{\mathscr{a}}^{\mathscr{Z}} U_{\mathscr{a},t}^{\mathscr{Z}} \le P_{\mathscr{a},t}^{\mathscr{Z}} \le \Omega_{\mathscr{a}}^{\mathscr{Z}} U_{\mathscr{a},t}^{\mathscr{Z}}\ \forall \mathscr{a}, \forall t \tag{35}$$

$$P_{\mathscr{a},t-1}^{\mathscr{Z}} - P_{\mathscr{a},t}^{\mathscr{Z}} > UR_{\mathscr{a}}^{\mathscr{Z}} \text{ if } P_{\mathscr{a},t-1}^{\mathscr{Z}} > P_{\mathscr{a},t}^{\mathscr{Z}}\ \forall \mathscr{a}, \forall t \tag{36}$$

$$P_{\mathscr{a},t-1}^{\mathscr{Z}} - P_{\mathscr{a},t}^{\mathscr{Z}} > DR_{\mathscr{a}}^{\mathscr{Z}} \text{ if } P_{\mathscr{a},t-1}^{\mathscr{Z}} < P_{\mathscr{a},t}^{\mathscr{Z}}\ \forall \mathscr{a}, \forall t \tag{37}$$

$$Q_{\mathscr{a},t}^{\mathscr{Z}} = P_{\mathscr{a},t}^{\mathscr{Z}} \sqrt{1 - \left(f_{\mathscr{a}}^{\mathscr{Z}}\right)^2} / f_{\mathscr{a}}^{\mathscr{Z}}\ \forall \mathscr{a}, \forall t \tag{38}$$

$$C_{\mathscr{a},t}^{\mathscr{Z}} = \left(\alpha_{\mathscr{a}}^{\mathscr{Z}} P_{\mathscr{a},t}^{\mathscr{Z}\,2} + \beta_{\mathscr{a}}^{\mathscr{Z}} P_{\mathscr{a},t}^{\mathscr{Z}} + \zeta_{\mathscr{a}}^{\mathscr{Z}}\right) U_{\mathscr{a},t}^{\mathscr{Z}}\ \forall \mathscr{a}, \forall t \tag{39}$$

$$R^{\mathscr{Z}} = \sum_{t=1}^{N_T}\sum_{\mathscr{a}=1}^{N_D}\left(P_{\mathscr{a},t}^{\mathscr{Z}} \pi_t^{\mathscr{S},m} - C_{\mathscr{a},t}^{\mathscr{Z}}\right) \tag{40}$$

$$\mathscr{E}^{\mathscr{Z}} = \sum_{t=1}^{N_T}\sum_{\mathscr{a}=1}^{N_D} P_{\mathscr{a},t}^{\mathscr{Z}} e_{\mathscr{a}}^{\mathscr{Z}}\ \forall \mathscr{a}, \forall t \tag{41}$$

where the active power $P_{\mathscr{a},t}^{\mathscr{Z}}$ of generator $\mathscr{a} \in \{1 : N_D\}$ is limited by its maximum capacity $\Omega_{\mathscr{a}}^{\mathscr{Z}}$ and minimum capacity $\mho_{\mathscr{a}}^{\mathscr{Z}}$ in (35) when the fuel-based DG is operating (i.e., the binary variable $U_{\mathscr{a},t}^{\mathscr{Z}} = 1$). Increasing and decreasing ramping constraints of DG units are modelled in (36) and (37), given the maximum increasing rate $UR_{\mathscr{a}}^{\mathscr{Z}}$ and decreasing rate $DR_{\mathscr{a}}^{\mathscr{Z}}$. It is assumed that generators can provide reactive power $Q_{\mathscr{a},t}^{\mathscr{Z}}$ based on (38) while operating at a constant power factor $f_{\mathscr{a}}^{\mathscr{Z}}$. Fuel consumption cost of DGs units $C_{\mathscr{a},t}^{\mathscr{Z}}$ is calculated in (39) as a function of generating power of units where $\alpha_{\mathscr{a}}^{\mathscr{Z}}$, $\beta_{\mathscr{a}}^{\mathscr{Z}}$ and $\zeta_{\mathscr{a}}^{\mathscr{Z}}$ are units' fuel consumption coefficients. The total profit of units $R^{\mathscr{Z}}$ is calculated in (40) in which the first term refers to the revenue from selling power, and the second term refers to the fuel cost. Then, the total emission of the DG unit $\mathscr{E}^{\mathscr{Z}}$ is determined in (41) by having $P_{\mathscr{a},t}^{\mathscr{Z}}$ and fuel-to-emission rate $e_{\mathscr{a}}^{\mathscr{Z}}$.

2.6. Grid operation

The operation of the grid is subjected to several operational constraints as follows:

2.6.1. Distribution power flow

Power flow equations for active and reactive powers are defined in (42-a) and (42-b):

$$P_i = \sum_{j=1}^{N_B} \Gamma_i \Gamma_j Y_{i,j} cos\left(\Theta_{i,j} - \delta_i + \delta_j\right) \forall i \tag{42-a}$$

$$Q_i = -\sum_{j=1}^{N_B} \Gamma_i \Gamma_j Y_{i,j} sin\left(\Theta_{i,j} - \delta_i + \delta_j\right) \forall i \tag{42-b}$$

where N_B is the number of buses, P_i, Q_i, Γ_i, and δ_i are the injected active power, injected reactive powers, voltage amplitude, and voltage angle at the bus i, respectively. $Y_{i,j}$ and $\Theta_{i,j}$ are the amplitude and angle of the $(i,j)^{th}$ entry of the bus admittance matrix [9].

2.6.2. Voltage limit of distribution buses

$$\Gamma_{Min} \le \Gamma_i \le \Gamma_{Max} \tag{43}$$

In order to reach a secure operation of the grid, the voltage of buses is limited to an acceptable operational voltage range $[\Gamma_{min}, \Gamma_{max}]$ for each bus i.

2.6.3. Power limit of distribution lines

$$\left|P_{i,j}^{line}\right| \le P_{i,j,Max}^{line} \tag{44}$$

Similar to voltage limits, as stated in (434), the power flow of the line $P_{i,j}^{line}$ between bus i and j is limited to a maximum power $P_{i,j,Max}^{line}$ due to the thermal capacity of branches.

2.6.4. Power balance

$$\sum_{\mathscr{g}=1}^{N_Y} P_{\mathscr{g},t}^{\mathscr{G}} + \sum_{\mathscr{a}=1}^{N_D} P_{\mathscr{a},t}^{\mathscr{Z}} + \sum_{c\in C_B}\sum_{m=1}^{\overline{\mathscr{T}}_{t,c}} P_{m,t,c}^{\mathscr{G},\mathscr{D}} + P_t^{\mathscr{S}} = P_t^{\mathscr{D}M} + P_t^{\mathscr{L}S} + \sum_{c\in C_B}\sum_{m=1}^{N_{M,c}} P_{m,t,c}^{\mathscr{G},\mathscr{C}} \forall t \tag{45}$$

The hourly power balance equation between the generation-demand of DN is modeled in [15]. $P_t^{\mathscr{S}}$ is the amount of power provided by the substation, $P_t^{\mathscr{D}M}$ is the hourly total load demand of the grid, and $P_t^{\mathscr{L}S}$ is the hourly total power loss of the grid and calculated in (446).

$$P_t^{\mathscr{L}S} = \sum_{i=1}^{N_B}\sum_{j>i}^{N_B} G_{ij}\left[\begin{array}{c}\Gamma_{i,t}^2 + \Gamma_{j,t}^2 - \\ 2\Gamma_{i,t}\Gamma_{j,t} cos\left(\delta_{i,t} - \delta_{j,t}\right)\end{array}\right] \tag{46}$$

where G_{ij} is the branch conductance between i^{th} and j^{th} buses. Using the distributed generators and storage system, the DSO aims to supply demands locally; however, the surplus/shortage powers are sold to/purchased from the upstream grid ($P_t^{\mathscr{S}}$).

2.6.5. Distributed resources modeling

In general, P-V and P-Q power flow models are used for DG in grid operation. This study considers DGs (both solar and fuel-based) as PQ nodes in which their generated powers are modeled as negative loads in power flow formulations.

2.7. Objective functions

The objective functions *Obj* of this paper include the total profit of DSO $R^{\mathscr{D}SO}$, total power loss $P^{\mathscr{L}S}$, total energy not supplied (ENS) *ENS*, and voltage stability index *VSI* of the grid as follows:

$$Opt\{Obj\} = [\max R^{\mathscr{D}SO}, \min P^{\mathscr{L}S}, \min ENS, \min VSI] \tag{45}$$

$$R^{\mathscr{D}SO} = R^{\mathscr{M}\mathscr{G}} + R^{\mathscr{G}} + R^{\mathscr{Z}} - \sum_{t=1}^{N_T} \left(P_t^{\mathscr{D}M} + P_t^{\mathscr{D}S}\right)\pi_t^{\mathscr{D},b} \quad (46)$$

$$P^{\mathscr{D}S} = \sum_{t=1}^{N_T} P_t^{\mathscr{D}S} \quad (47)$$

$$ENS = \sum_{t=1}^{N_T}\sum_{i=1}^{N_B-1} \zeta_i L_i \left[\sum_{k\in \mathrm{ll}_i} Pd_{t,k}\left(r_k^s + r_k^r\right)\right] \quad (48)$$

$$VSI_t = \frac{1}{N_B}\sum_{j=1}^{N_B} VSI_{j,t} \quad (49)$$

DSO uses DGs and storage units to reduce the power loss and power purchase from the upstream grid (46); otherwise, DSO needs to supply demands at the day-ahead market price $\pi_t^{\mathscr{D},b}$. The second objective is to minimize total power loss (47). In the *ENS* formulation (48), as the third objective, switching-time r_k^s and repair-time r_k^r are considered when the branch i is not available because of a failure, where ll_i denotes the set of buses not supplied when bus i is disconnected, and $Pd_{t,k}$ is amount of unsupplied load at buses ll_i. A failure rate ζ_i and length L_i are assumed for each of the branches. Minimizing voltage stability index in (49) is the last objective function in which $VSI_{j,t} = SCC_{j,t}^{min}/SCC_{j,t}$. The Thevenin-equivalent circuit method in [27] is adopted to calculate the minimum short circuit current corresponding to marginal voltage stability index $SCC_{j,t}^{min}$, and the short circuit current at each bus $SCC_{j,t}$. Finally, the objective value of $VSI = \max(\{VSI_1, VSI_2, \cdots, VSI_t\})$.

3. Case study and results

In this study, the proposed methodology is applied to IEEE 33-bus and IEEE 136-bus DN to assess the effectiveness of utilizing MCAESs in terms of given objectives. Swarm robotics search & rescue [28] is used as the optimization algorithm. Different scenarios of load variations are given in [1]. Hourly price of the energy and realistic data of solar power production is based on the Australian electricity market for 20th April 2020 [29]. The selling price is 10 % lower than the purchase price. Four different cases (corresponding to given objective functions) are presented for each scenario.

3.1. IEEE 33-bus system

3.1.1. Scenario 1: Solar and fuel-based DG units

As the base case, this scenario investigates the involvement of solar and diesel units. Four solar units with the capacity of 400 kW, 600 kW, 800 kW, and 1000 kW, are located at buses 10, 18, 26, and 32, respectively. The specifications of the DGs are presented in Table 1. A power factor of 0.9 is considered for all DGs (solar and fuel-based). In terms of ENS calculation, the failure rate is $\zeta_i = 0.05$ for all lines and length L_i is based on distance matric $\mathfrak{D}_{i,j}$. Two situations of the single fault and double fault are considered for each hour.

3.1.2. Scenario 2: Solar, fuel-based DGs, and stationery CAESs

In this scenario, the stationary form of CAESs is also added to the grid. Specifications of CAES units are detailed in Table 2. The proposed forward–backward approach has been employed in this case, though the location matrix formulation is not used for tanks since storage units are stationary in this scenario. The user-defined factors of energy mismatch ϵ^g is 1 kW and termination criterion ϵ^δ is 50 in this paper. Location of CAESs is considered as decision variable.

Table 1
Specification of DG units.

Type	1	2	3	4
Min capacity [kW]	100	150	200	200
Max capacity [kW]	500	750	1000	1000
Location bus	16	18	31	33
Fuel factors $\alpha_{\mathscr{d}}^{\mathscr{Z}}\left[\$/\mathrm{kW}^2\right]$, $\beta_{\mathscr{d}}^{\mathscr{Z}}$ [$/kW], $\zeta_{\mathscr{d}}^{\mathscr{Z}}$ [$]	5.8E-6, 0.21, 0	5.8E-6, 0.21, 0	5.3E-6, 0.20, 0	5E-6, 0.20, 0
Emission factor [g/kWh]	695	695	477	625

Table 2
Specification of MCAES units.

Parameter of motor-generator (MGs)	Value	Parameter of storage tanks	Value
Number of MGs	6	Number of tanks per MG	3
Maximum charging capacity of MGs [kW]	200	Capacity per tank [kWh]	200
Maximum discharging capacity of MGs [kW]	200	Initial idle hours of tanks	0
Charging/discharging stability rate of MGs	5 %	Maximum depth of discharge	95 %
Power factor	1	Average speed of trucks [km/h]	65
Charging/discharging efficiency	0.85	Initial energy per tank [kWh]	100

3.1.3. Scenario 3: Solar units, fuel-based DGs, and MCAESs

This scenario is an extended form of the previous scenario in which the location matrix of moving tanks is determined based on the proposed methodology. The fuel consumption of rigid trucks carrying tanks and the price of diesel fuel are assumed based on the Survey of Motor Vehicle Use, Australia [30].

3.1.4. Comparison of the results

In Scenario 1, fuel-based DGs need to compensate for the lack of energy produced by solar units during the first and last hours of the day to improve the voltage of buses to an acceptable range. The results of this scenario for different objectives are detailed in Table 3. A negative value for the ENS factor means that the total summation of generation during the 24 h scheduling horizon is more than the corresponding load demand considering different scenarios of fault/failure. Similarly, operation profit has negative values since the DSO needs to buy energy from day-ahead markets. Although values of a specific objective for two or more cases are rather close (e.g., power loss in Cases 1 and 4), as they are very different in profit, ENS, and VSI.

In Scenario 2, stationary CAES units are added to the system. Scheduling results for the given configuration are detailed in Table 4. As can be seen, compared to the results of Scenario 1, the value of objective functions is improved for different cases. Unlike fuel-based DGs that generate energy, stationary storage systems only take advantage of price changes and are not highly efficient for power loss improvement because they increase the power loss during the charging period relatively at the same amount they reduce during discharging. In terms of operating profit, CAES can provide some benefit for the first three cases even though objectives are different for cases 2 & 3. However, the CAES unit significantly improves voltage stability in case 4, where a stability index of 0.5983 is achieved.

For Scenario 3, stationary CAESs are replaced by MCAES technology. The results of different cases for this scenario are presented in Table 5.

Table 3
Optimum results for different objectives (Scenario 1).

Case num.	Objective	Operating profit [$]	Power loss [kWh]	ENS single; double fault/s [kWh]	VSI
1	$\max R^{\mathscr{D}SO}$	−15,059.39	1372.9	−3,721.26; 512,200.26	0.7533
2	$\min P^{\mathscr{D}S}$	−15,748.32	989.33	2,077.48; 559,425.95	0.7217
3	min*ENS*	−15,415.25	1463.13	−6,328.27; 499,304.21	0.7927
4	min*VSI*	−15,763.48	1346.82	5,509.76; 596,426.23	0.6685

Table 4
Optimum results for different objectives (Scenario 2).

Case num.	Objective	Operating profit [$]	Power loss [kWh]	ENS single; double fault/s [kWh]	VSI
1	max$R^{\mathscr{DSO}}$	−14,346.67	1,501.09	−5942.42; 505,850.66	0.7447
2	min$P^{\mathscr{DS}}$	−14,863.88	1,004.28	2,190.20; 71,943.27	0.7311
3	min*ENS*	−14,975.01	1,578.68	−9,175.74; 473,740.43	0.6879
4	min*VSI*	−15,490.74	1,326.02	3,301.22; 590,735.83	0.5983

Table 5
Optimum results for different objectives (Scenario 3).

Case num.	Objective	Operating profit [$]	Power loss [kWh]	ENS single; double fault/s [kWh]	VSI
1	max$R^{\mathscr{DSO}}$	−14,477.46	1,417.68	−2,940.04; 561,571.70	0.7176
2	min$P^{\mathscr{DS}}$	−15,067.08	970.92	1,732.26; 561,571.70	0.7136
3	min*ENS*	−15,238.32	1,579.18	−9302.16; 473,828.68	0.6408
4	min*VSI*	−15,603.11	1,318.05	2,309.82; 577,409.26	0.5641

As it can be seen from this table, MCAES technology can improve the operating condition of the grid in terms of total power loss, ENS, and VSI; however, operating profit in Scenario 3 cannot reach a better value than that of Scenario 2. Thus, DSO can operate the grid using stationary CAES technology in normal condition with the objective of profit maximization. To further improve the reliability/ resilience or VSI correction of the grid after an event, DSO can simply switch from stationary CAES to MCAES.

Fig. 1. shows details of operating profits for Scenario 1 – Scenario 3. In this figure, the purchased energy includes base-load demand plus active power loss of the corresponding case. Besides, tradable energy includes power generation from solar units, fuel-based DGs, and stationary/mobile CAESs. The solar and fuel-based DGs have a major role in power selling based on the hourly load profile, and the CAES units provide additional profit by reducing the expensive commitment of fuel-based DGs. The lack of locational marginal price causes mobile technology to be unable to take advantage of price changes at different locations. Additionally, the fuel cost of MCAES is the reason for reducing the total profit in Scenario 3. In terms of power loss, MCAES provides a small improvement while offering a considerable profit improvement in Scenario 3 compared to Scenario 1. As can be seen from Fig. 2, MCAESs are highly efficient for ENS improvement compared to Scenario 1. Compared to Scenario 2, the hourly ENS value is improved during only some hours, even though its total value is lower in Scenario 3. The histogram for 24 h voltage of the grid in Scenario 3 is shown in Fig. 3. It can be seen that Case 4 has the lowest divergence from the desired mean value of 1 p.u. This situation provides DSO with a safe zone against significant sudden changes of loads in the grid, although selecting this objective results in a higher operational cost based on Table 5.

The total charge/discharge pattern of energy at the location of generators of MCAES units are shown in Fig. 4. Since there is no significant solar generation for hours in which the price of energy is high, fuel-based DGs and storage units are the only sources of power provision. In such a situation, the load will be supplied by CAES units if the energy price is around 35 % higher than the price during the charging time (i.e., because $1/\ (\alpha_c^{\mathscr{G},\mathscr{C}} \times \alpha_c^{\mathscr{G},\mathscr{D}})$ where $\alpha_c^{\mathscr{G},\mathscr{C}} = \alpha_c^{\mathscr{G},\mathscr{D}} = 0.85$); otherwise, fuel-based DGs are the only option for the power supply.

Hourly generation of fuel-based DGs in Scenario 3 is depicted in Fig. 5. The maximum total amount of fuel-based DGs' generation happens in Case 3, where the energy provision of units directly affects the amount of ENS in the grid. For Case 2, fuel-based DGs tend to maximize profit by charging mobile tanks during low energy price hours and discharging during high energy price hours. Therefore, energy generation from the most expensive fuel-based DGs is minimized.

3.2. IEEE 136-bus system

For this case study, the proposed methodology has been applied to the standard IEEE 136-bus system. The same scenarios and objective

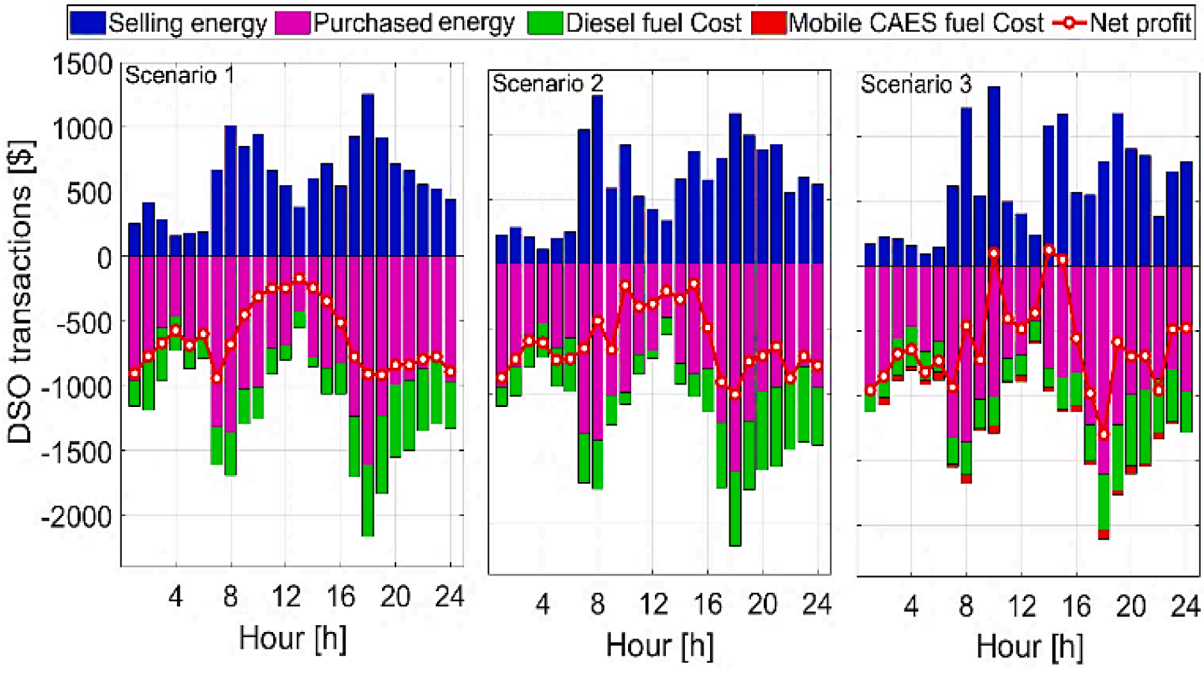

Fig. 1. Hourly financial transactions of DSO - Case 1 (Scenarios 1– 3).

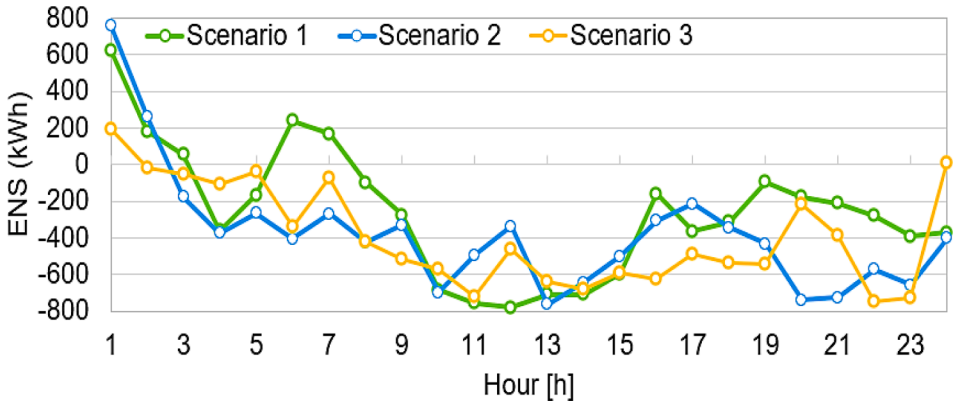

Fig. 2. Hourly single-fault ENS profile (Case 3) for Scenarios (1–3).

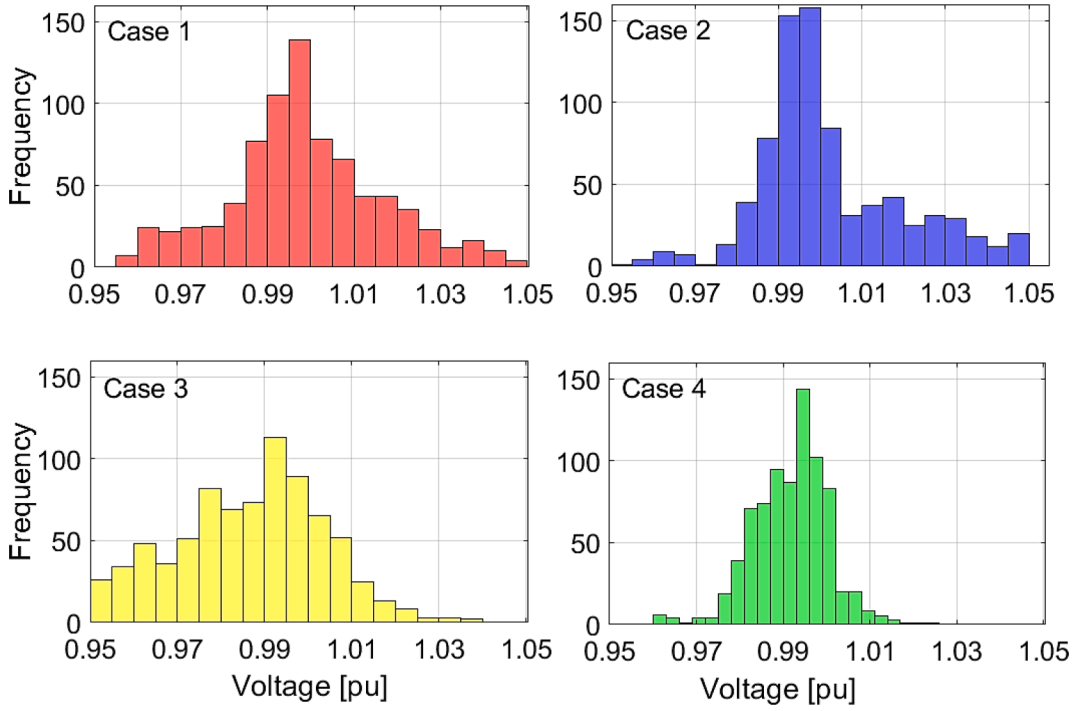

Fig. 3. Histogram for voltage profile of buses (different cases- Scenario 3).

cases have been considered for this test system. The number of solar units, fuel-based DGs, and MCAES generators has increased to 12, 9, and 11 units, respectively, while the number of tanks per MCAES unit has remained the same. Results for the given scenarios are detailed in Tables 6-8. As can be seen, increasing the grid scale has made the impact of MCAES technology utilization more significant in several cases. Considering the grid is geographically spread over a much larger area, the reliability factor ENS is significantly decreased in comparison to Scenario 2. The ENS objective function values have been reduced from 89,483.83 (for single fault) and 19, 174,498 (for double faults) to 54,029.83 (for single fault) and 16,212,038 (for double faults), respectively. Similarly, the notable applicability of MCAES for voltage stability enhancement of the network is much more apparent in this test system compared to stationary CAES, as the VSI value has remarkably been reduced from 0.4991 to 0.3823. As noted, the lower mean value of VSI indicates that the system is more stable. It is also revealed that IEEE 136-bus system is more stable as compared to IEEE 33-bus system.

Evidently, results demonstrate that the transportability of MCAES is more beneficial in larger DNs to decrease the active power loss of the grid. In terms of the operating profit, even though MCAES could reach a substantial improvement compared to the base-case scenario, it still provides a lower profit than stationary CAES. With all these above considerations, it is clear that the MCAES is a better choice for a large-scale network in the sense of reduced power loss and ENS, and increased profitability and stability.

4. Conclusions

This paper studies the application of MCAES technology in the DN network. The obtained results demonstrate that adding MCAES technology to the grid can significantly improve the operating performance of the grid (3.86 % in net profit, 1.85 % in power loss, 31.97 % in single fault ENS, and 15.61 % in VSI for the IEEE 33-bus system). These performance indicators are better than the results of using stationary CAES (except net profit), owing to the high dispatchability of MCAES technology using inexpensive mobile air storage tanks. It would be a potential option for DSO to switch between stationary and mobile modes to reach an extra 1.98 % profit. Additionally, the case study for the large 136-bus system shows more obvious benefits of MCAES (6.75 % in net profit, 4.47 % in power loss, 39.62 % in single fault ENS, 23.40 % in

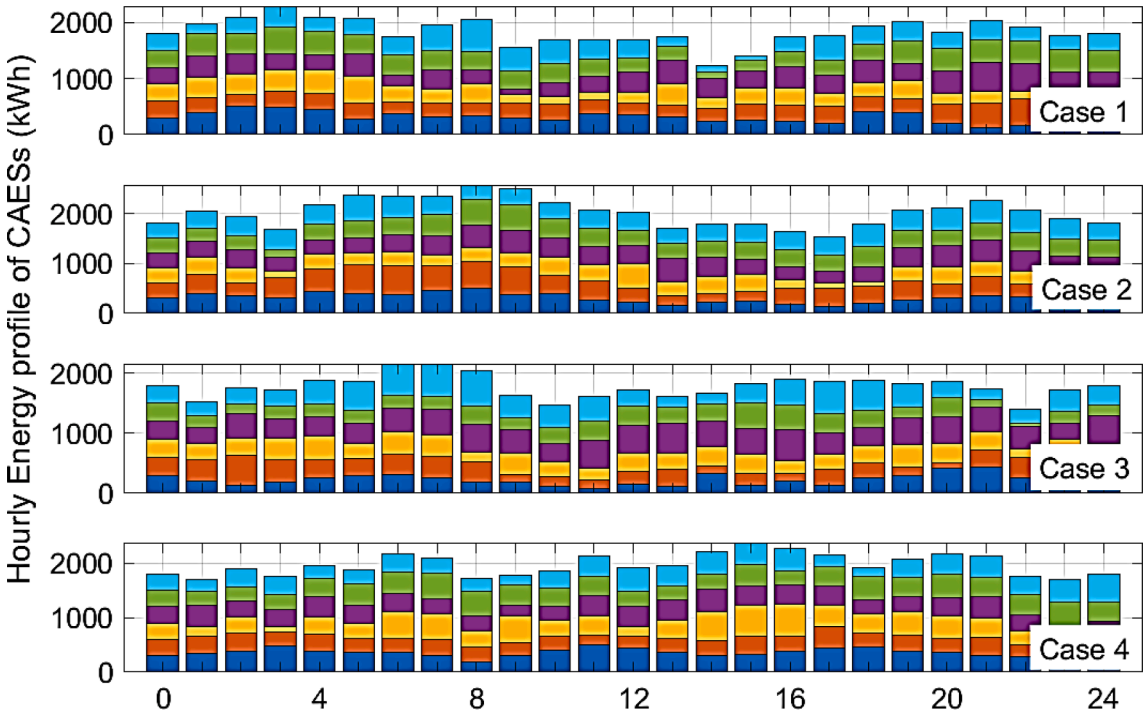

Fig. 4. The total hourly variations of energy for CAES units (Scenario 3).

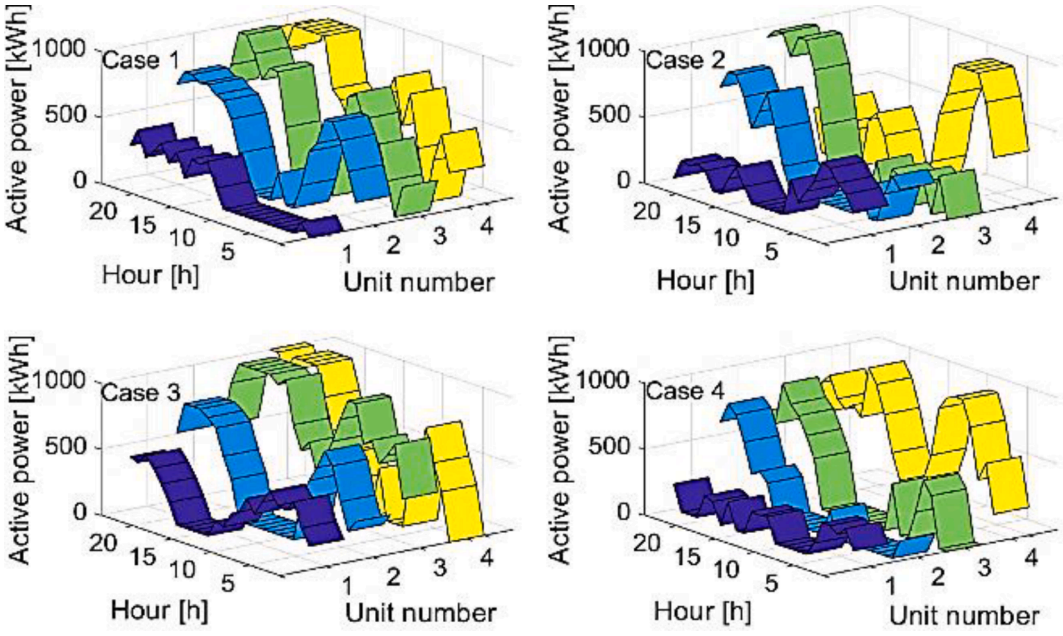

Fig. 5. Active generation of fuel-based DGs in different cases (Scenario 3).

VSI). Hence, the geographical dimensionality of the grid has a notable effect on the applicability of the MCAES. Besides, MCAES has shown significant improvement for grids that suffer heavily from periodic voltage instability and critical events Moreover, a lower commitment to fuel-based DGs has been obtained with the help of MCAESs, which also contributes to a lower amount of emission. The presented forward–backward approach for constraint handling of MCAES units, along with the proposed solution coding, has largely reduced the dimension, complexity, and computational burden of the solution approach. Using the updated data from Google Maps API has also removed the challenges related to route congestion modeling and model linearization for optimal movements of storage units.

Electric vehicles (EVs) are one of the most important competitors of MCAESs. Currently, there is significant research ongoing to aggregate and employ EVs to facilitate distribution grid services. However, EVs have lower accessibility and shorter life cycle (battery degradation) compared with MCAESs. Indeed, CAESs are featured by their economic feasibility, large capacity, low environmental impact and long life. Considering these factors, MCAES can be used in smart grids, spinning reserve black start applications, and supply shortages due to intermittencies.

This research can be further extended to the following applications:

Table 6
Optimum results for different objectives considering IEEE 136-bus system (Scenario 1).

Case num.	Objective	Operating profit [$]	Power loss [kWh]	ENS single; double fault/s [kWh]	VSI
1	max$R^{\mathscr{DSO}}$	−83,622.45	4,469.43	93,036.74; 19,482,653	0.5661
2	min$P^{\mathscr{TS}}$	−86,444.44	4,155.87	95,380.70; 19,211,786	0.5237
3	min*ENS*	−89,847.09	4,594.61	89,483.83; 19, 174,498	0.5785
4	min*VSI*	−91,598.21	4,289.50	108,162.41; 19,956,241	0.4991

Table 7
Optimum results for different objectives considering IEEE 136-bus system (Scenario 2).

Case num.	Objective	Operating profit [$]	Power loss [kWh]	ENS single; double fault/s [kWh]	VSI
1	max$R^{\mathscr{DSO}}$	− 76,975.54	4,492.23	89,758.89; 19,117,132	0.5167
2	min$P^{\mathscr{TS}}$	−77,670.80	4,113.03	97,043.63; 19,351,856	0.5002
3	min*ENS*	−78,908.34	4,565.98	67,794.97; 17,065,303	0.4716
4	min*VSI*	−80,515.47	4,290.11	100,131.23; 19,749,275	0.4469

Table 8
Optimum results for different objectives considering IEEE 136-bus system (Scenario 3).

Case num.	Objective	Operating profit [$]	Power loss [kWh]	ENS single; double fault/s [kWh]	VSI
1	max$R^{\mathscr{DSO}}$	−78,012.28	4,419.09	91,736.19; 19,232,839	0.4518
2	min$P^{\mathscr{TS}}$	−79,328.02	3,969.87	94,185.46; 19,184,954	0.4159
3	min*ENS*	−79,864.39	4,501.54	54,029.83; 16,212,038	0.3989
4	min*VSI*	81,001,27	4,282.30	93,279.13; 19,635,249	0.3823

- CAES can be applied in virtual power plants to improve market profit and reliability.
- CAES can also be applied to an integrated demand response program to provide an alternative method of energy storage and generation.
- CAES can be applied in military operations to provide necessary power supplies in forward bases. Mobile CAES can also be applied to increase distribution system resilience under natural disasters. A multi-level risk-constraint energy scheduling approach for trading in the day-ahead and real-time electricity market can also be studied in the future.
- Integration of small-scale CAES with solar roof-top generation for flexible household power supply can be studied in the future.

The number of pilot studies about small-scale CAES in distribution grids are very limited at this stage.

- It is expected that real-world applications of CAES will receive much more attention in the near future.

CRediT authorship contribution statement

Mojtaba Jabbari Ghadi: Investigation, Software. **Dillip Kumar Mishra:** Data curation, Visualization. **Ali Azizivahed:** Methodology. **Li Li:** Supervision, Resources. **Jiangfeng Zhang:** Validation, Conceptualization.

Declaration of Competing Interest

The authors declare that they have no known competing financial interests or personal relationships that could have appeared to influence the work reported in this paper.

Data availability

No data was used for the research described in the article.

References

[1] Ghadi MJ, et al. Day-Ahead Market Participation of an Active Distribution Network Equipped with Small-Scale Compressed Air Energy Storage Systems. IEEE Trans Smart Grid 2020.
[2] Jadidbonab M, et al. "Risk-constrained energy management of PV integrated smart energy hub in the presence of DR and compressed air energy storage. IET Renew Power Gener, vol. 13, no. 6, 2019.
[3] Guo Z, et al. "Operation of Distribution Network Considering Compressed Air Energy Storage Unit and Its Reactive Power Support Capability. IEEE Trans Smart Grid, vol. 11, no. 4, 2020.
[4] Cheng J, et al. Dispatchable Generation of a Novel Compressed-Air Assisted Wind Turbine and Its Operation Mechanism. IEEE Trans Sustain Energy 2018;10(4): 2201–10.
[5] Zhang J, et al. A bi-level program for the planning of an islanded microgrid including CAES. IEEE Trans Ind Appl 2016;52(4):2768–77.
[6] Abdulnasser G, Ali A, Shaaban MF, Mohamed EE. Stochastic multi-objectives optimal scheduling of energy hubs with responsive demands in smart microgrids. J Storage Mater 2022;55:105536.
[7] Ghadi MJ, et al. Application of small-scale compressed air energy storage in the daily operation of an active distribution system. Energy 2021;231:120961.
[8] Dai R, Esmaeilbeigi R, Charkhgard H. The utilization of shared energy storage in energy systems: A comprehensive review. IEEE Trans Smart Grid 2021;12(4): 3163–74.
[9] Abdeltawab HH, Mohamed YA.-RI. "Mobile energy storage scheduling and operation in active distribution systems." IEEE Trans Ind Electron, vol. 64, no. 9, 2017.
[10] Liu X, Soh CB, Zhao T, Wang P. Stochastic scheduling of mobile energy storage in coupled distribution and transportation networks for conversion capacity enhancement. IEEE Trans Smart Grid 2020;12(1):117–30.
[11] Arteaga J, Zareipour H. A price-maker/price-taker model for the operation of battery storage systems in electricity markets. IEEE Trans Smart Grid 2019;10(6): 6912–20.
[12] Hosseini SS, Badri A, Parvania M. A survey on mobile energy storage systems (MESS): Applications, challenges and solutions. Renew Sustain Energy Rev 2014; 40:161–70.
[13] Wang W, Xiong X, He Y, Hu J, Chen H. Scheduling of separable mobile energy storage systems with mobile generators and fuel tankers to boost distribution system resilience. IEEE Trans Smart Grid 2021;13(1):443–57.
[14] Abdeltawab H, Mohamed Y-A-R-I. Mobile Energy Storage Sizing and Allocation for Multi-Services in Power Distribution Systems. IEEE Access 2019;7:176613–23.
[15] Srivastava A, et al., "Minimizing Cost of Smart Grid Operations by Scheduling Mobile Energy Storage Systems." IEEE Lett Comput Soc, vol. 2, no. 3, 2019.
[16] Song Y, et al., "Multi-objective configuration optimization for isolated microgrid with mobile energy storage and shiftable load." In: *2018 IEEE Conference on Energy System Integration* 2018: IEEE, pp. 1-7.
[17] Yao S, Wang P, Zhao T. Transportable energy storage for more resilient distribution systems with multiple microgrids. IEEE Trans Smart Grid 2018;10(3):3331–41.
[18] Mishra DK, Ghadi MJ, Li L, Zhang J, Hossain M. Active distribution system resilience quantification and enhancement through multi-microgrid and mobile energy storage. Appl Energy 2022;311:118665.
[19] Kim J, Dvorkin Y. Enhancing distribution system resilience with mobile energy storage and microgrids. IEEE Trans Smart Grid 2018;10(5):4996–5006.
[20] Chen Y, Zheng Y, Luo F, Wen J, Xu Z. Reliability evaluation of distribution systems with mobile energy storage systems. IET Renew Power Gener 2016;10(10):1562–9.
[21] Tao Y, Qiu J, Lai S, Dong ZY. Transportable Energy Storage System Planning for Mitigating Grid Vulnerability. IEEE Trans Power Syst 2022.
[22] Yao S, et al., "Two-stage stochastic scheduling of transportable energy storage systems for resilient distribution systems." In: *2018 IEEE International Conference on PMAPS*, 2018: IEEE, pp. 1-6.
[23] Prabawa P, Choi D-H. "Multi-Agent Framework for Service Restoration in Distribution Systems With Distributed Generators and Static/Mobile Energy Storage Systems." *IEEE Access,* vol. 8, 2020.

[24] Saboori H, Jadid S. Optimal scheduling of mobile utility-scale battery energy storage systems in electric power distribution networks. J Storage Mater 2020;31:101615.
[25] Kwon S-Y, et al. Optimal V2G and Route Scheduling of Mobile Energy Storage Devices Using a Linear Transit Model. IEEE Trans Ind Appl 2019;56(1):34–47.
[26] Nazemi M, Dehghanian P, Lu X, Chen C. Uncertainty-aware deployment of mobile energy storage systems for distribution grid resilience. IEEE Trans Smart Grid 2021;12(4):3200–14.
[27] Azizivahed A, Narimani H, Naderi E, Fathi M, Narimani MR. A hybrid evolutionary algorithm for secure multi-objective distribution feeder reconfiguration. Energy 2017;138:355–73.
[28] Bakhshipour M, Ghadi MJ, Namdari F. Swarm robotics search & rescue: A novel artificial intelligence-inspired optimization approach. Appl Soft Comput 2017;57:708–26.
[29] Market Data National Energy Market (NEM) Web [Online] Available: https://www.nemweb.com.au/.
[30] Eisapour AH, Naghizadeh A, Eisapour M, Talebizadehsardari P. Optimal design of a metal hydride hydrogen storage bed using a helical coil heat exchanger along with a central return tube during the absorption process. Int J Hydrogen Energy 2021;46(27):14478–93.